A Compact CSRR Enabled UWB Diversity Antenna

Muhammad Saeed Khan, *Student Member, IEEE,* Antonio-D-Capobianco, *Member, IEEE,* Sajid M. Asif, *Student Member, IEEE,* Dimitris E. Anagnostou, *Senior Member, IEEE,* Raed M. Shubair, *Senior Member, IEEE,* Benjamin D. Braaten, *Senior Member, IEEE*

***Abstract*— The purpose of this paper is to introduce a compact Ultra-Wideband (UWB) diversity antenna with a very low Envelope Correlation Coefficient (ECC). The design employs a hybrid isolation enhancing and miniaturization technique. The antenna consists of two counter facing monopoles, and is miniaturized by using not only inverted-L stubs but also a Complementary Split Ring Resonator (CSRR) on the ground plane. The added components enhance isolation and enable tighter packing of the antennas. The result is a very compact MIMO array with an overall size of 23 x 29 mm^2, that covers the entire UWB spectrum from 3 GHz to 12 GHz, with mutual coupling lower than -15 dB. Moreover, the CSRR unit that acts as a resonator is applied for the first time to suppress the interference of RF currents flowing through the ground plane of this UWB MIMO/diversity antenna. The performance of the fabricated prototype in terms of scattering parameters, broadside (peak) gain, radiation patterns, efficiency and envelope correlation coefficient is presented and discussed.**

***Keywords*- Filter, antenna arrays, Complementary split ring resonator (CSRR), continuous spectrum, integrated components, monopole radiator, Multiple-Input-Multiple-Output (MIMO).**

I. Introduction

Although Ultra-Wideband (UWB) technology can provide wide bandwidth communications with low energy levels, it is vulnerable to interference including multipath fading [1]. To mitigate this problem, UWB technology can be combined with Multiple-Input-Multiple-Output (MIMO) technology to provide the multiplexing gain and diversity gain that will improve the link quality and capacity of a communications system [2]. A UWB-MIMO antenna consists of at least two radiating elements with low mutual coupling between them. To achieve the low coupling, the elements can be placed at a certain distance, but in portable devices the available space is usually very limited.

Diversity antennas have traditionally employed various methods to maintain the total antenna size compact [3]-[8]. Many of these works employed perpendicularly placed monopoles. For example, in [3] Ren et al. etched slots on the monopoles to enhance their isolation. Also, in [4], L. Liu et al. increased the bandwidth and isolation of the monopoles by adding stubs on the ground plane. A rectangular stub on the ground for an asymmetric coplanar strip (ACS)-fed antenna was proposed in [5] by Y. F. Liu et al. Another technique to enhance the isolation was introduced by Khan et al. [6-7] and involved a parasitic decoupling structure on the ground plane. A neutralization line has also been inserted on the ground plane to increase isolation, as presented by Wang et al. [8]. Also, a perpendicular feeding network has been used by Adamiuk et al. to reduce mutual coupling [9]. A common denominator in all these approaches is the ubiquitous trade-off between bandwidth, size and design complexity.

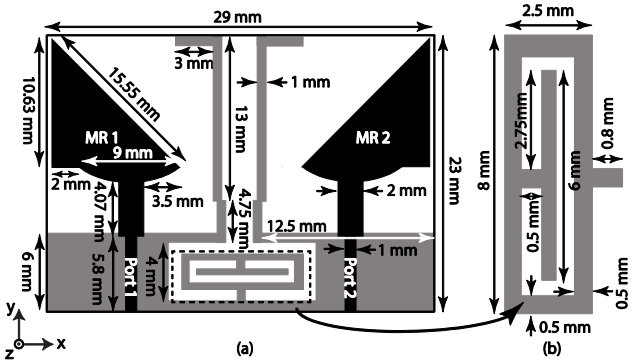

Fig. 1: Geometry of the proposed UWB MIMO antenna system. (a) Layout with dimensions and (b) CSRR unit with dimensions.

In this paper, an UWB MIMO/diversity antenna with a 3 to 12 GHz bandwidth is presented. The design which is shown in Fig. 1, is novel in terms of its hybrid isolation enhancement and miniaturization technique. First, two stubs are added on the ground plane between the two antennas to further enhance the isolation in the range 3.6 to 12 GHz. The stubs also improved the impedance matching. Next, a complementary split ring resonator (CSRR) is placed on the ground plane to enhance the isolation below 3.6 GHz. The principles of operation of the stubs and the CSRR will be explained in the following. The proposed design results in the most compact and smallest UWB diversity antenna that is currently available in literature. The proposed radiator consists of two triangular monopoles that are placed adjacent to each other, leading to an antenna with total dimensions of 23mm × 29mm = 667 mm^2, which is 18% smaller than the design proposed by Y. F. Liu et al. [5], ca. 2014, which is one of the smallest ever reported.

II. Design Concepts

The design steps of the MIMO antenna are shown in Fig. 2. To explain the hybrid miniaturization method, the effects of the stubs and CSRR on the bandwidth and mutual coupling are described next.

M. S. Khan and A. D. Capobianco are with the Department of Information Engineering of Padova University, Padova, 35100, Italy.

M. S. Khan is also with the Department of Electrical Engineering, COMSATS Institute of IT, Pakistan (e-mail:mskj786@hotmail.com).

S. M. Asif and B. D. Braaten are with the Department of Electrical and Computer Engineering, North Dakota State University, Fargo, ND 58102 USA. S. M. Asif is also with the Department of Electrical Engineering, COMSATS institute of IT, Attock, Pakistan.

D. E. Anagnostou is with the South Dakota School of Mines & Techn. Rapid City, SD 57701 USA and also with Heriot-Watt University, Edinburgh, UK (e-mail:danagn@ieee.org).

R. M. Shubair is with both Electrical and Computer Engineering Department at Khalifa University, UAE and Research Laboratory of Electronics of Massachusetts Institute of Technology (MIT), USA (email: rshubair@mit.edu).

The authors acknowledge financial support from the University of Padova, project CPDA150022.

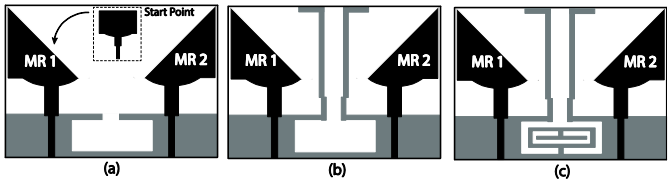

Fig. 2: Geometry of the proposed UWB/MIMO with ground variations. (a) Without CSRR and stubs (b) with two stubs and (c) with CSRR and stubs.

Initially, a rectangular shaped UWB radiator was designed according to the guidelines given in literature [10], this was later modified to triangular shaped and ground plane dimensions to achieve the wide-band matching. Also, a second triangular monopole was placed near to it as shown (Fig. 1(a)) that share the same ground plane. By using triangular shapes (instead of rectangular ones as shown in Fig. 2(a)), the monopoles do not face (and radiate) directly towards each other, which allowed the first reduction in the spacing between the two elements. Each monopole is fed with a 50 Ω microstrip feed line. As expected, when the two triangular antennas are placed side by side (Fig. 2(a)), they do not exhibit good impedance matching in the entire UWB range. There is impedance mismatch from 6.8 to 8.4 GHz (Fig. 3(a)) and poor isolation from 3 to 6.8 GHz (Fig. 3(b)). It is worth noting that a good diversity MIMO antenna requires a mutual coupling less than -15 dB.

Two inverted L-shaped stubs are then inserted in the ground plane to enhance isolation and (as seen by the result) improve the matching by acting as wavetraps [11] and adding resonances. The shapes of these stubs are modified from the straight inverted L-shaped to segmented inverted L-shaped stubs because the positions of these stubs have a huge effect on the antenna properties. The stubs have a total length of $\lambda_0/4$ (λ_0 at 3.8 GHz) and serve a dual purpose. First they act as reflectors [4] that separate the radiation of the monopoles and therefore reduce mutual coupling. This can be seen from Fig. 3b, where stubs increase the isolation to more than 12dB over the entire UWB bandwidth. The second purpose is that they also act as radiators and introduce two resonances, one at 3.8 GHz and the other one at 6.8 GHz as shown in Fig. 3(a). These resonances help particularly to improve the matching in the previously-mismatched range, resulting in a well-matched antenna over the entire UWB range. They also help in increasing isolation in the same frequency range, as shown in Fig. 3(b). Moreover, the lower resonance at 3.8 GHz also shifts the lower cutoff of the antenna to 2.5 GHz in simulation, which provides a promising safety limit for the fabricated prototype. It is noteworthy that by changing the length of the inverted L-shaped stubs, the resonances can be shifted to lower or higher frequencies. Also, by adding more stubs, more resonances can be obtained.

Despite having achieved a satisfactory impedance matching bandwidth from 2.5 to 12 GHz, the isolation at the lower end of the UWB range (from 3 to 3.6 GHz) remained low. To increase the isolation at such a low frequency, larger stubs (4mm longer than the current stub) would be needed thus increasing significantly the overall size of the antenna. For this reason, a CSRR was inserted in the ground plane to maintain the size of the antenna as compact as possible, as shown in Fig. 2(c). The CSRR acts as an LC tank circuit resonator that

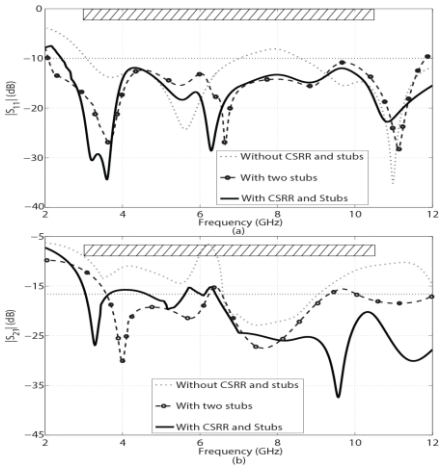

Fig. 3: (a) Simulated $|S_{11}|$ and (b) Simulated $|S_{21}|$, to illustrate the effect of the introduced stubs and of the CSRR on improving the antenna bandwidth and reducing the mutual coupling to below -15 dB.

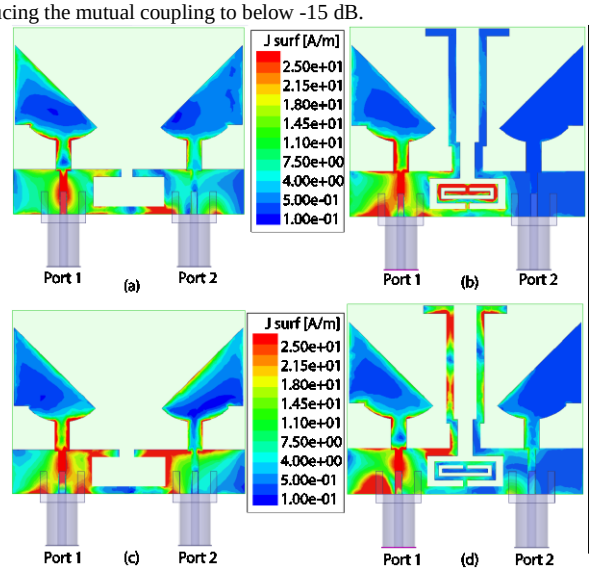

Fig. 4: Surface current distribution with and without CSRR and Stubs. (a,b) at 3.45 GHz and (c,d) at 6 GHz. Only port 1 is excited .The plot illustrates how the stubs and CSRR resonator reduce the coupling between the two elements. Notice that in (Figs. 4b and d) there is very little current on the second (right) antenna from port-1 when the stubs and the CSRR have been introduced.

stores the low frequency energy and 'traps' the current of the ground, preventing it from reaching the other element. The CSRR length and width are originally designed to introduce a resonance at 3.45 GHz, a frequency that is later shifted higher when the CSRR is integrated in the ground plane with the entire antenna structure. However, these CSRR characteristics, as also noted by Baena et al. [12], prevent most of the current from flowing between the two antennas and significantly increase the antenna isolation. Here, the CSRR improved the isolation from 3 to 3.9 GHz, resulting in achieving the necessary 3 to 12 GHz isolation bandwidth as also shown in Fig. 3(b).

To investigate further the combined effect of the stubs and the CSRR, the surface current distribution at 3.45 and 6 GHz was observed. The above two frequencies are selected because of their proximity to the resonances that the CSRR and stubs produce. Without the CSRR and stubs (Fig. 4a), when port-1 (only) is excited at 3.45 GHz, the current is strongly coupled to port-2 and high mutual coupling is observed between the radiators. When the CSRR and stubs are inserted, the amount

of the current that is coupled to port-2 is about 20 times smaller, with most of the current being trapped in the CSRR, as shown in Fig. 4(b). Additional simulations showed that most of the 6 GHz current is trapped on the stubs that act as wave-traps [12], which explains also the reduced coupling (S_{21}) that is observed in Fig. 3(b).

In Table I, a comparison of the proposed antenna with the most representative UWB-MIMO antennas presented in literature is shown. The list is not comprehensive but fairly represents the current state-of-the-art of this technology. The proposed antenna is compact and has almost the same or better features as other antennas possess.

TABLE I
PERFORMANCE COMPARISON WITH PREVIOUS PUBLISHED LITERATURE

Published literature	Total PCB size (mm^2)	Band-width (GHz)	Mutual coupling (dB)	Gain Var-(dBi)/ Total efficiency (%)	ECC using far-field patterns
[6] Khan	33 x 45.5	3.1-10.6	<- 15	**2.3/85**	< 0.6
[3] J. Ren	32 x 32	3.1-10.6	< -15	2.5/60	N.A
[16] Khan	23 x 39.8	2.5-12	**<-21**	2.8/82	< 0.6
[5] Y. F. Liu	28.5 x 28.5	2.66 to 10.8	< -15	2.2/N.A	N. A
[14] Zhang	35 x 40	3.0-10.6	< -15	3.1/N.A	N.A
Proposed antenna	**23 x 29**	**3-12**	< - 15	4.7/82	**< 0.15**

III. RESULTS AND DISCUSSION

A. S-parameters

The proposed antenna was printed on a Rogers TMM4 1.524 mm thick substrate with a dielectric permittivity of ε_r = 4.5 and loss tangent tanδ = 0.002. The S-parameters of the prototype (shown in Fig. 5) were measured with an Agilent E5071C network analyzer and the results matched well with the simulations, as shown in Fig. 6. The antenna covers the 3 to 12 GHz bandwidth with $|S_{11}|$ < -10 dB, and with $|S_{12}|$ < -15 dB. A short cable with ferrite bead rings to suppress the flow of RF current on the outside was used in the measurements. There is a slight mismatch between simulations and measurements at the lower frequencies, possibly due to the proximity of the large connectors and cable to the antenna.

B. Radiation Patterns

The radiation patterns at three representative frequencies (3.5 GHz, 7 GHz, and 10.5 GHz) in the principal planes *x-z* (*H*-plane) and *y-z* (*E*-plane), were measured in the anechoic chamber and compared with the simulations. At the lower frequency (3.5 GHz), the measured gain patterns are slightly smaller than the simulated (Fig. 7(a)), possibly due to a small portion of the RF current flowing back from the antenna onto the outer surface of the short feeding cable [13]. This is also validated later in Fig. 8, where the effect of the cable in the reduction of the gain at the lower frequencies is evident. At higher frequencies (7.0 and 10.5 GHz), where the cable appears to have a smaller effect, the measured gain patterns are closer to the simulated ones. Most important, a near-omnidirectional pattern is maintained in the H-plane, even at the higher frequencies (7.0 GHz and 10.5 GHz). During the measurements, port-1 was excited and port-2 was terminated with a matched load. When port 2 is excited, the patterns in the *y-z* plane are similar but the patterns in the *x-z* plane are mirrored transformations about the *y-z* plane.

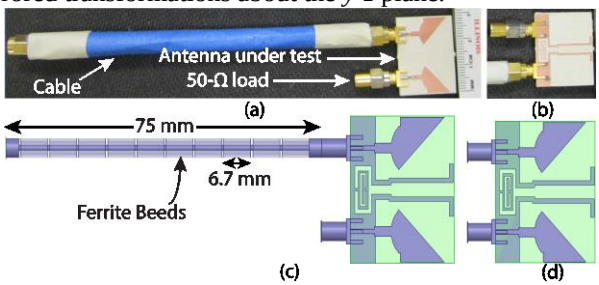

Fig. 5: Photo of the developed prototype with the short feeding cable used in the simulation and measurements (a) top side of fabricated prototype and (b) bottom side of fabricated prototype and (c) simulated model in HFSS with short feeding cable and (d) simulated model in HFSS without cable.

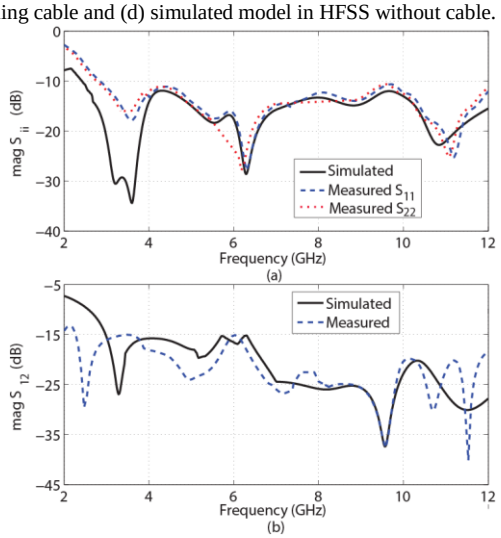

Fig. 6: Simulated and measured (a) $|S_{ii}|$ and (b) $|S_{21}|$, illustrating a good performance of the fabricated device, similar to the simulated.

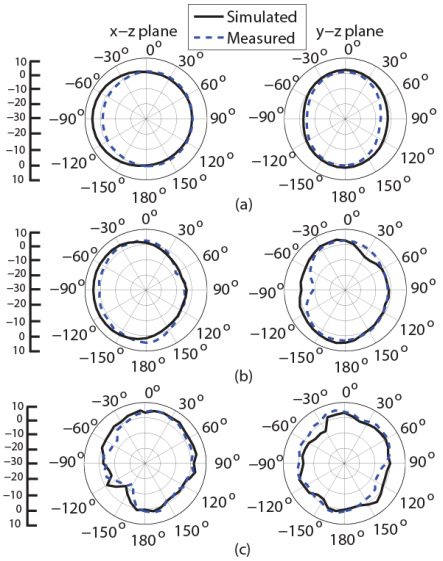

Fig. 7: Simulated and measured radiation pattern (a) 3.5 GHz and (b) 7 GHz and (c) 10.5 GHz, exhibiting near-omnidirectional radiation suitable for UWB-MIMO systems.

C. GAIN AND EFFICIENCY

For a fair evaluation of the gain and efficiency of the antenna, the cable effect and losses were taken into account by modelling the cable in HFSS, as shown in Fig. 5(c). The total

This article has been accepted for publication in a future issue of this journal, but has not been fully edited. Content may change prior to final publication. Citation information: DOI 10.1109/LAWP.2016.2520401, IEEE Antennas and Wireless Propagation Letters

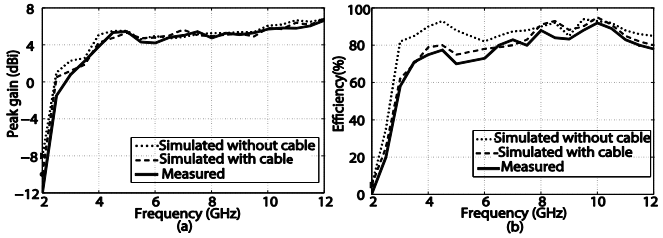

Fig. 8: (a) Simulated and measured peak gain and (b) Simulated and measured efficiencies. The antenna is efficient over the entire spectrum. The effect of the cable on the gain and the efficiency at the lower frequencies is evident.

length of the cable used in simulation and measurement was 75 mm. Ten ferrite beads were used on the cable and the length of each ferrite bead was approximately 6.7 mm. The peak antenna gain is shown in Fig. 8(a). The measured gain varies from 1.2 to 5.9 dBi over the UWB spectrum, and the measured efficiency (shown in Fig. 8(b)) matched the simulated efficiency with the cable. A good agreement with the measured results was observed, noting that the measured efficiency of the antenna with the cable connected was less than the simulated without cable (above 82%), particularly at the lower frequencies, which was anticipated for the reasons explained in Section III.B.

D. Diversity Analysis

In MIMO systems, when two or more antenna elements exhibit different radiation patterns in a plane, then these elements can be used to mitigate the effects of multipath. In the proposed MIMO antenna, both elements have the same patterns in the *y-z* plane but in the *x-z* plane, the patterns are mirror images of each other, as explained in Section III.B. Moreover, the *x-y* plane patterns are mirror images of each other (as also shown in Fig. 9). For example, in Fig. 9(a), antenna MR1 has a null at 60° while antenna MR2 has a 0 dBi gain at that angle. Similarly, antenna MR2 has the null 'mirrored' at 120°, which is where MR1 has a gain of 0 dBi. At the higher frequency of 7.0 GHz, both radiators have a main lobe at opposite sides (180° difference angle) while MR1 has a null at 30° and MR2 has a null at -150°. As a conclusion, these patterns are reasonably uncorrelated, and the envelope correlation coefficient (ECC) ρ_e, using simulated 3-D radiation patterns was numerically calculated by using Eqn. (7) in [14]:

$$\rho_e = \frac{\left|\int_0^{2\pi}\int_0^{\pi}\left(XPR\cdot E_{\theta 1}\cdot E_{\theta 2}^{*}\cdot P_{\theta}+E_{\varphi 1}\cdot E_{\varphi 2}^{*}\cdot P_{\varphi}\right)d\Omega\right|^2}{\int_0^{2\pi}\int_0^{\pi}\left(XPR\cdot E_{\theta 1}\cdot E_{\theta 1}^{*}\cdot P_{\theta}+E_{\varphi 1}\cdot E_{\varphi 1}^{*}\cdot P_{\varphi}\right)d\Omega\times\int_0^{2\pi}\int_0^{\pi}\left(XPR\cdot E_{\theta 2}\cdot E_{\theta 2}^{*}\cdot P_{\theta}+E_{\varphi 2}\cdot E_{\varphi 2}^{*}\cdot P_{\varphi}\right)d\Omega} \quad (1)$$

where XPR is the cross-polarization ratio, and P_θ and P_φ are the θ and φ components of the angular density functions of the incoming wave. The calculated ECC values from the simulated patterns are lower than 0.15, over the complete spectrum, which indicates that the proposed antenna is well suited for diversity applications.

IV. Conclusion

A hybrid miniaturization technique was proposed for very compact UWB-MIMO/diversity antennas. The method was applied successfully on an example prototype antenna with two radiating monopoles, and the measured performance validated the usefulness of the miniaturization concepts. To enhance the isolation among the radiators, two inverted L-shaped stubs were used on the ground plane on the back side

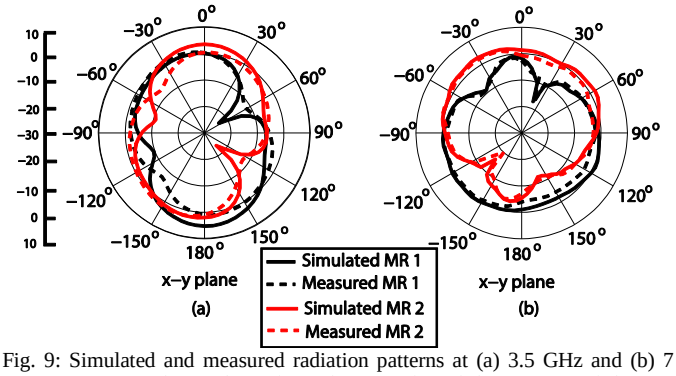

Fig. 9: Simulated and measured radiation patterns at (a) 3.5 GHz and (b) 7 GHz, in the *x-y* plane. The 'mirrored' properties of the patterns of the two antennas can be observed.

of the antenna. Moreover, to keep the antenna compact and obtain the desired isolation at the lower frequencies, a CSRR unit was integrated in the ground plane. Results show that the antenna has very low coupling extending beyond the entire UWB frequency range (3 to 12 GHz). The small size of only 23 x 29 mm^2, the omni-directional radiation characteristics, and the diversity analysis make the proposed antenna an excellent candidate for portable UWB-MIMO systems.

References

[1] R. Vaughan and J. Anderson, "Antenna diversity in mobile application-ns," *IEEE Trans. on Vehicular Tech.*, vol. 36, no. 4, pp. 149- 172, 1987.

[2] L. Zheng and C. Tse, "Diversity and multiplexing: A Fundamental Trade-off in Multiple Antenna Channels," *IEEE Trans. Inf. Theory*, vol. 49, pp. 1073-1096, May 2003.

[3] J. Ren et al, "Compact Printed MIMO Antenna for UWB Applications," *IEEE Antenna wireless propag. Lett.*, vol. 13, pp. 1517-1520, 2014.

[4] L. Liu, S. W. Cheung and T. I. Yuk, "Compact MIMO Antenna for Portable devices in UWB Applications," *IEEE Trans. Antennas Propag.*, vol. 61, no. 8, pp. 4257-4264, Aug. 2013.

[5] Y. F. Liu et al, "Compact ACS-fed UWB Antenna for Diversity Appl-ications," *IET Electron. Lett.*, vol. 50, no. 19, pp. 1336-1338, Sep. 2014.

[6] M. S. Khan et al, "Compact Ultra-wideband Diversity Antenna with a Floating Parasitic Digitated Decoupling Structure," *IET Microwaves, Antenna and Propag.*, Mar, 2014.

[7] M. S. Khan et al, "Isolation enhancement of a wideband MIMO antenna using Floating Parasitic Elements," *Microwave Optical and Technology Letters*, vol. 57, no. 7, pp. 1677-1682, July, 2015.

[8] Y. Wang and Z. Du, "A wideband printed dual-antenna system with a novel neutralization line for mobile terminals," *IEEE Antenna wireless propag. Lett.*, vol. 12, pp. 1428-1431, 2014.

[9] G. Adamiuk et al, "Dual-orthogonal polarized antenna for UWB-IR tec-hnology," *IEEE Ant. Wireless Propag. Lett.*, vol. 8, pp. 981-984, 2009.

[10] M. S. Khan et al, "Compact UWB-MIMO Antenna Array with a Novel Decoupling Structure," *IEEE International Bhurban Conference on Applied Science and Technology (IBCAST)*, pp. 347-350, Jan. 2013.

[11] P. Lindberg and E. Ojefors, "A bandwidth enhancement technique for mobile handset antennas using wavetraps", *IEEE Trans. Antennas and Propagation*, vol. 54, no. 8, pp.2226 – 2233, Aug. 2006.

[12] J. D. Baena et al, "Equivalent circuit models for split ring resonators and complementary split ring resonators coupled to planar transmission lines," *IEEE Trans. Micr. Theory & tech.*, vol. 53, pp. 1451-1461, 2005.

[13] L. Liu, S. W. Cheung, Y. F. Weng, T. I. Yuk and M. A. Matin, "Cable effects on measuring small planar UWB monopole antenna," *Ultra Wideband- Current Status and Future Trends*, Oct. 2012.

[14] M. B. Knudsen and G. F. Pedersen, "Spherical outdoor to indoor power spectrum model at the mobile terminal," *IEEE J. Sel. Areas Communic.*, vol. 20, no. 6, pp. 1156- 1168, Aug. 2002.

[15] S. Zhang et al, "Ultrawide band MIMO/Diversity Antennas With a Tree-Like Structure to Enhance Wideband Isolation," *IEEE antennas and wireless propagation letters*, vol. 8, pp. 1279-1282, 2009.

[16] M. S. Khan et al, "Planar, Compact Ultra-Wideband Polarisation Diversity Antenna Array," *IET Microwaves, Antennas and Propagation*, vol. 9, no. 15, pp.1761-17688, Dec., 2015.